




Level-density parameters in superheavy nuclei

A. Rahmatinejad, A. N. Bezbakh, T. M. Shneidman ^{*}, G. Adamian, and N. V. Antonenko
Joint Institute for Nuclear Research, Dubna 141980, Russia

P. Jachimowicz 
Institute of Physics, University of Zielona Góra, Szafrana 4a, 65516 Zielona Góra, Poland

M. Kowal [†]
National Centre for Nuclear Research, Pasteura 7, 02-093 Warsaw, Poland



(Received 18 May 2020; accepted 19 February 2021; published 9 March 2021)

We systematically study the nuclear level densities of superheavy nuclei, including odd systems, using the single-particle energies obtained with the Woods-Saxon potential diagonalization. We applied minimization over many deformation parameters for the global minima-ground states, and the “imaginary water flow” technique on a many-deformation energy grid for the saddle points, including nonaxial shapes. The level density parameters are calculated by fitting the obtained results with the standard Fermi gas expression. The total potential energy and shell correction dependencies of the level-density parameter are analyzed at the ground state and saddle point. These parameters are compared with the results of a phenomenological approach. As shown, this expression should be modified for the saddle points, especially for small excitation energy. The ratio of the level-density parameter at the saddle point to that at the ground state is shown to be crucial for the survival probability of a heavy nucleus.

DOI: [10.1103/PhysRevC.103.034309](https://doi.org/10.1103/PhysRevC.103.034309)

I. INTRODUCTION

Considerable progress in the experimental synthesis of new superheavy nuclei has been achieved recently [1,2], and further experiments on producing heavier elements are planned with the constructed new “superheavy factory” at the Joint Institute for Nuclear Research (JINR). The success in production of superheavy nuclei mainly depends on how strongly a hot compound nucleus, created in a complete fusion reaction, is opposed to the fission process. Thus, the survival probability, which takes into account the competition between neutron emission and fission, plays an important role in the formation of evaporation residues. The relative importance of these two decay modes mainly depends on the corresponding level densities. To estimate which of the decay processes wins this competition, one should know the level densities at the ground states and at the fission saddle points. Moreover, the height and position of the saddle point are crucial for estimation of survival probability of an excited compound nucleus.

To calculate level densities, one can determine all eigenvalues, with their degeneracy, of the nuclear Hamiltonian and then count how many of them are in the energy interval of interest. Because the total number of states exponentially increases with excitation energy above several MeV, the problem becomes treatable only statistically. There are a number

of sophisticated combinatorial methods to do this; see for example Refs. [3,4] where the parity, angular momentum, pairing correlations, as well as collective enhancements are explicitly treated based on the Gogny interaction. As shown in Ref. [5], there is a general and exact scheme to calculate the particle-hole level densities for an arbitrary single-particle Hamiltonian taking into account the Pauli exclusion principle. The role of microscopic level densities during the fission process and their effect on the evolution of the nuclear shapes and on the distribution of excitation energies can be found in [6–9]. Nuclear level densities calculated within the relativistic mean-field theory are shown in [10]. Single-particle level densities for various temperatures using a self-consistent mean-field approach are determined in [11] while in [12] level density parameters are calculated with help of the Yukawa-folded potential. The spin- and parity-dependent shell-model nuclear level densities obtained with the moment method in the proton-neutron formalism are presented in Ref. [13]. Direct microscopic calculation of nuclear level densities in the shell model Monte Carlo approach is presented in Ref. [14]. In practical applications we still must use a number of approximations and assumptions, and even corrections such as superfluidity effect or collective rotational and vibrational enhancement.

Ultimately, the most important value in practical applications is the empirical level-density parameter a , which is studied in this article. One should remember that the level density at the saddle is not the same as that at the ground state. Indeed, the energy available for occupation of the levels at the

^{*}Also at Kazan Federal University, Kazan 420008, Russia.

[†]michal.kowal@ncbj.gov.pl

saddle point is lowered by the difference in the deformation energy between the saddle and ground states. Another reason is that the single-particle levels are distributed differently due to the change of geometrical shape of the compound nucleus. It is therefore crucial to find the right saddle point that governs the fission process. To find all saddle points on energy hypercube and then choose the proper one between them is quite a demanding task.

Based on the fact that going from low to higher energies the nuclear system reverts from a paired system to a system of noninteracting fermions, one can successfully describe it with the well-known Fermi-gas model. In this phenomenological model, the pairing effect is taken into account with a constant parameter Δ . In the Fermi-gas model, the average value of the level-density parameter, which establishes the connection between the excitation energy and nuclear temperature, is often assumed to depend linearly on the mass number A [15]. In real situation, the level-density parameter is energy dependent and gradually reaches an asymptotic value with increasing energies above the neutron separation energy. The phenomenological expression was introduced in Ref. [16] to determine the energy and shell correction dependencies of the level-density parameter.

The main goal of this paper is to combine the state-of-the-art methods: the imaginary water flow technique on a many-deformation space for saddles and multidimensional minimization for ground states with the statistical approach for calculation of level-density parameters at those extreme (saddle and minima) points. We use the BCS model to calculate the intrinsic level densities of superheavy nuclei with $Z = 112, 114, 116, 117, 118$, and 120 . As is known, this formalism is successful in description of nuclear quantities such as level density and isomeric ratio [17]. The ratio of the level density parameter at the saddle point to that at the ground state is important to calculate the survival probability of an excited heavy nucleus. This ratio will be considered with the energy dependence of neutron emission probability from excited heavy and superheavy nuclei.

II. METHOD OF CALCULATION

We apply a two-step approach for level calculation. In the first step, using the macroscopic-microscopic (MM) method, we determine all necessary minima and saddle points. The minima are calculated by using multidimensional minimization while the saddle points by applying the imaginary water flow technique (IWF) on multidimensional energy grids. In the second stage, we use the statistical formalism allowing us to estimate the level-density parameters at these extreme points, employing the deformed single-particle spectra. Having these results, competition between fission and neutron emission is evaluated.

A. Ground states and saddle points

To calculate the potential energy surfaces, the MM method is used. In the frame of this method the microscopic energy is calculated by applying the Strutinski shell and pairing correction method [18] with the single-particle levels obtained

after diagonalization of the deformed Woods-Saxon potential [19]. The $n_p = 450$ lowest proton levels and $n_n = 550$ lowest neutron levels from the $N_{max} = 19$ lowest shells of the harmonic oscillator are taken into account in the diagonalization procedure. The standard values of $\hbar\omega_0 = 41/A^{1/3}$ MeV for the oscillator energy and $\gamma = 1.2\hbar\omega_0$ for the Strutinski smearing parameter, and a six-order correction polynomial are used in the calculation of the shell correction. For the macroscopic part, we use the Yukawa plus exponential model [20] with the parameters specified in Ref. [21]. The deformation dependent Coulomb and surface energies are integrated by using the 64-point Gaussian quadrature.

For nuclear ground states, based on our previous tests and results [22–24], we confined our analysis to axially symmetric shapes parametrized by spherical harmonics expansion of the nuclear radius truncated at β_{80} :

$$R(\vartheta) = cR_0\{1 + \beta_{20}Y_{20} + \beta_{30}Y_{30} + \beta_{40}Y_{40} + \beta_{50}Y_{50} + \beta_{60}Y_{60} + \beta_{70}Y_{70} + \beta_{80}Y_{80}\}, \quad (1)$$

where the dependence of spherical harmonics on ϑ is suppressed and c is the volume-fixing factor depending on deformation. In this case, the energy is minimized over seven degrees of freedom specified in (1), by using the conjugate gradient method. To avoid falling into local minima, the minimization is repeated dozens of times for each nucleus, with randomly selected starting deformations. For odd systems, the additional minimization over configurations is performed at every step of the gradient procedure.

Triaxial and mass-asymmetric deformations are included and the IWF method is used for finding the saddles. This allows us to avoid errors inherent in the constrained minimization approach [25–28]. This very efficient technique in the study of fission barriers was first applied in Ref. [29]. To find saddles, the energy for each nucleus is calculated on the five-dimensional (5D) deformation grid and then fivefold interpolated in each dimension for the IWF search.

So, in order to find the proper first saddle point we use a five-dimensional deformation space, with the expansion of the nuclear radius

$$R(\vartheta, \varphi) = cR_0\left\{1 + \beta_{20}Y_{20} + \frac{\beta_{22}}{\sqrt{2}}[Y_{22} + Y_{2-2}] + \beta_{40}Y_{40} + \beta_{60}Y_{60} + \beta_{80}Y_{80}\right\}, \quad (2)$$

where the quadrupole nonaxiality β_{22} is explicitly included. For each nucleus we generate the following 5D grid of deformations:

$$\begin{aligned} \beta_{20} &= 0.00 (0.05) 0.60, \\ \beta_{22} &= 0.00 (0.05) 0.45, \\ \beta_{40} &= -0.20 (0.05) 0.20, \\ \beta_{60} &= -0.10 (0.05) 0.10, \\ \beta_{80} &= -0.10 (0.05) 0.10 \end{aligned} \quad (3)$$

of 29 250 points (nuclear shapes); the numbers in the parentheses specify the grid steps. Additionally, for odd and odd-odd nuclei, at each grid point we look for low-lying

configurations blocked by particles on levels from the tenth below to the tenth above the Fermi level. Then, our primary grid (3) was extended by the fivefold interpolation in all directions. Finally, we obtained the interpolated energy grid of more than 5×10^6 points. To find the first saddles on such a giant grid, we use the IWF method (see, e.g., [30,31]). The most important properties of both ground states and saddle points of heaviest nuclei with $98 < Z < 126$ and $134 < N < 192$, obtained within our MM method, have been collected recently in extended tables of Ref. [32].

B. Level-density parameters

Based on the superconducting formalism [33], the constants (G_N and G_Z) of the pairing interaction for neutrons and protons are adjusted to obtain the ground-state pairing gaps (Δ_N and Δ_Z) of the MM method with the following equations:

$$N = \sum_k \left(1 - \frac{\varepsilon_{N,k} - \lambda_N}{E_{N,k}} \tanh \frac{\beta E_{N,k}}{2} \right), \quad (4)$$

$$\frac{2}{G_N} = \sum_k \frac{1}{E_{N,k}} \tanh \frac{\beta E_{N,k}}{2} \quad (5)$$

for neutrons and

$$Z = \sum_k \left(1 - \frac{\varepsilon_{Z,k} - \lambda_Z}{E_{Z,k}} \tanh \frac{\beta E_{Z,k}}{2} \right), \quad (6)$$

$$\frac{2}{G_Z} = \sum_k \frac{1}{E_{Z,k}} \tanh \frac{\beta E_{Z,k}}{2} \quad (7)$$

for protons at zero temperature. The quasiparticle energies $E_{N(Z),k} = \sqrt{(\varepsilon_{N(Z),k} - \lambda_{N(Z)})^2 + \Delta_{N(Z)}^2}$ are calculated using the single-particle energies ($\varepsilon_{N(Z),k}$) of the Woods-Saxon potential. Using the obtained values of the pairing constants, the pairing gaps and chemical potentials ($\lambda_{N(Z)}$) are determined by solving Eqs. (4)–(7) at given temperatures ($T = 1/\beta$). Then, setting the obtained values in the following equations, the excitation energies ($U = U_Z + U_N$), entropies ($S = S_Z + S_N$), and intrinsic level densities (ρ) are calculated:

$$E_{Z,N}(T) = \sum_k \varepsilon_k \left(1 - \frac{\varepsilon_k - \lambda_{Z,N}}{E_k} \tanh \frac{\beta E_k}{2} \right) - \frac{\Delta_{Z,N}^2}{G_{Z,N}}, \quad (8)$$

$$U_{Z,N}(T) = E_{Z,N}(T) - E_{Z,N}(0), \quad (9)$$

$$S_{Z,N}(T) = 2 \sum_k \left\{ \ln[1 + \exp(-\beta E_k)] + \frac{\beta E_k}{1 + \exp(\beta E_k)} \right\}, \quad (10)$$

$$\rho = \frac{\exp(S)}{(2\pi)^{\frac{3}{2}} \sqrt{D}}, \quad (11)$$

where D is the determinant of the matrix composed of the second derivatives of the entropy with respect to β and $\mu = \beta\lambda$. The calculations were repeated using the single-particle level energies obtained with the Woods-Saxon potential at the saddle point. In the BCS calculations of the saddle point the pairing constants were taken from the ground-state results. Above the critical temperature (T_{cr}) the pairing gap

vanishes and all thermodynamical quantities revert to those of a noninteracting Fermi system. Generally, larger density of states close to the Fermi surface at the saddle point leads to larger pairing correlation and as a consequence larger value of the critical temperature in comparison to the ground state. In the mass region considered, the critical temperatures for neutrons and protons are up to 0.42 MeV at the ground state and 0.52 MeV at the saddle point. The corresponding total excitation energies are $U_{cr} \approx 5.14$ MeV at the ground state and $U_{cr} \approx 11.27$ MeV (with respect to the ground state) at the saddle point. Fitting the calculated values of intrinsic level density at an specified excitation energy with the back-shifted Fermi gas expression

$$\rho_{FG}(U) = \frac{\sqrt{\pi}}{12a^{\frac{1}{4}}(U - \Delta)^{\frac{5}{4}}} \exp(2\sqrt{a(U - \Delta)}), \quad (12)$$

one can obtain the level density parameter $a(U)$ as a function of excitation energy. In the calculations, the energy back-shifts are taken as $\Delta = 24/\sqrt{A}$, $12/\sqrt{A}$, and 0 MeV for even-even, odd, and odd-odd isotopes, respectively. Energy and shell correction (δE_{sh}) dependencies of the level density parameter can be described with the following phenomenological expression [16]:

$$a(A, U) = \tilde{a}(A) \left[1 + \frac{1 - \exp[-(U - \Delta)/E_D]}{U - \Delta} \delta E_{sh} \right], \quad (13)$$

where E_D is known as the damping parameter and indicates how the shell effect in the level-density parameter damps with increasing U . We would like to emphasise that we obtain the damping parameter and the asymptotic value \tilde{a} of the level density parameter by analyzing the calculated energy dependent level-density parameter with Eq. (13) for each considered nucleus separately. However, for practical reasons, we also want to stay at the phenomenological level. To do this one can find systematics of \tilde{a} as this value smoothly depends on the mass number (see Ref. [16])

$$\tilde{a} = \alpha A + \beta A^2. \quad (14)$$

The damping parameter in turn can be approximated as

$$E_D = A^{1/3} / \gamma_0. \quad (15)$$

Here, α , β , and γ_0 are the parameters providing the best fit of the calculated energy dependent level density parameters in the nuclei considered.

C. Survival probability

Finally, the most important seems to be the use of this formalism to estimate the probability of survival of the synthesized nucleus. The survival probability of heavy and superheavy nuclei is proportional to the ratio of neutron emission width (Γ_n) to fission width (Γ_f) [34]. This ratio is calculated as

$$\frac{\Gamma_n}{\Gamma_f} = \frac{gA^{2/3} \int_0^{U-B_n} \varepsilon \rho_{GS}(U - B_n - \varepsilon) d\varepsilon}{K_0 \int_0^{U-B_f} \rho_{SP}(U - B_f - \varepsilon) d\varepsilon}, \quad (16)$$

where g is the neutron intrinsic spin degeneracy, $K_0 \approx 10$ MeV [34], and B_n and B_f are neutron separation energy and

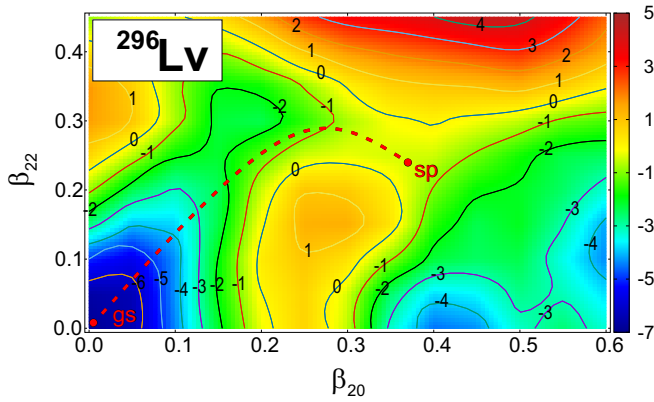


FIG. 1. Potential energy landscape projected onto the (β_{20}, β_{22}) plane for ^{296}Lv . The possible fission path is shown by the dashed line from the ground state (gs) to the saddle point (sp). Energy (in MeV) is calculated relative to the macroscopic energy at the spherical shape.

fission barrier height, respectively. Here, ρ_{GS} and ρ_{SP} are the level densities calculated at the ground state and saddle point, respectively. Based on the Fermi gas model, the following analytical expression of Γ_n/Γ_f can be obtained [34]:

$$\frac{\Gamma_n}{\Gamma_f} = \frac{4A^{2/3}a_f(U - B_n - \Delta_n)}{K_0a_n[2a_f^{1/2}(U - B_f - \Delta_f)^{1/2} - 1]} \times \exp[2a_n^{1/2}(U - B_n - \Delta_n)^{1/2} - 2a_f^{1/2}(U - B_f - \Delta_f)^{1/2}], \quad (17)$$

where Δ_f and Δ_n are the back-shifts in the Fermi gas level densities at the saddle point and ground state, respectively. Assuming only neutron emission and fission decay channels, the neutron emission probability is written as

$$\frac{\Gamma_n}{\Gamma_{\text{tot}}} = \frac{\Gamma_n/\Gamma_f}{1 + \Gamma_n/\Gamma_f}, \quad (18)$$

and is strongly affected by the ratio

$$\frac{a_f}{a_n} = \frac{a_{\text{SP}}(A, U - B_f)}{a_{\text{GS}}(A - 1, U - B_n)}, \quad (19)$$

which should be calculated and discussed for the superheavy nuclei considered.

III. RESULTS AND DISCUSSION

A. Proton and neutron single-particle spectra

As we want to compare the behavior of the level densities at saddles in relation to that at the ground state, we start with a description (giving an example) of their determination, which is crucial for further work. As mentioned in Sec. II, the determination of the fission barrier in multidimensional space requires hypercube calculations and application of the IWF technique on the hypercube. The potential energy surface for ^{296}Lv , as an example, is shown in Fig. 1 on the $(\beta_{20}; \beta_{22})$ plane obtained by minimizing energy on the five-dimensional grid (3) with respect to $\beta_{40}, \beta_{60}, \beta_{80}$. The landscape modification obtained by including quadrupole nonaxiality deformation β_{22} in (2) is important for the picture of the first saddle points.

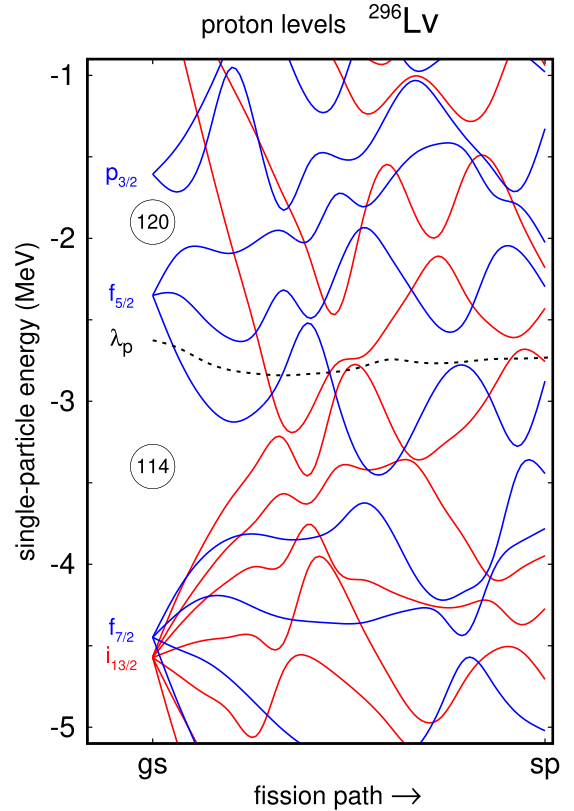


FIG. 2. Proton single-particle spectrum along the fission path for ^{296}Lv (see Fig. 1). The Fermi level is indicated by the dotted line.

The strong reduction of axial barrier, by about 2 MeV, due to this effect is clearly seen on the map. One should keep in mind that the energy mapping in multidimensional space becomes a problem. A reduction of dimension via the minimization over some deformations often leads to an energy surface composed of disconnected patches, corresponding to multiple minima in the auxiliary (those minimized over) dimensions. This is why the real saddle point found with the IWF technique in full deformation space may be located in a slightly different place than the one shown in Fig. 1. An example of a fission path starting from a nearly spherical ground state and ending on a triaxial saddle point is shown in Fig. 1 by a red dashed line. Along the fission path the orders of the Woods-Saxon single-particle levels are shown in Figs. 2 and 3 for protons and neutrons, respectively. The evolution of the Fermi level ($\lambda_{p(n)}$) is traced by black dotted lines in both cases.

Our calculations show that Eq. (13) for $a(A, U)$ gives a good agreement with the BCS calculations at the ground state, in which the values of the shell corrections are significant. This is fully supported by the single-particle spectra shown in Fig. 2 for protons and in Fig. 3 for neutrons, from which one can see the importance of shell effects. First, clearly visible is a well-known large energy gap for $Z = 114$ and a much smaller, although still distinct one for $Z = 120$ at the ground states. This obviously contributes to the significant value of the shell effect in the ground state. When approaching the saddle point the spectrum becomes more complicated with a lot of level crossings. However, it is clear that the single-

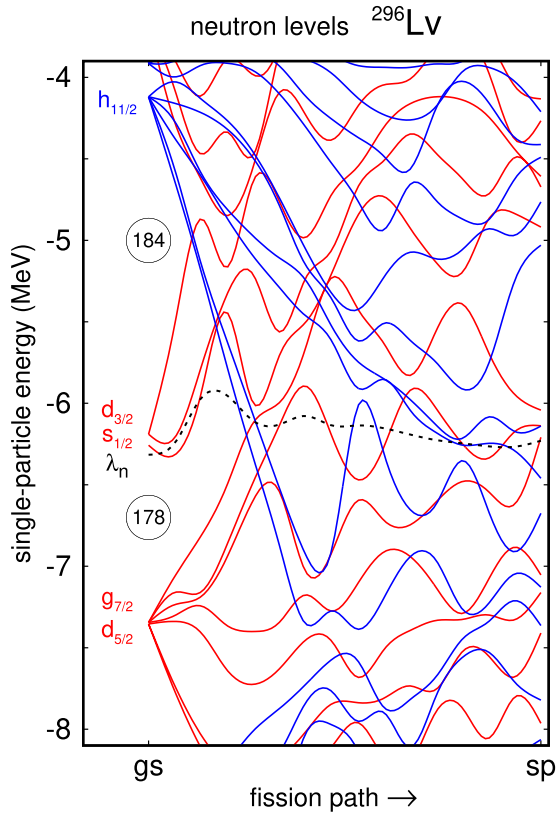


FIG. 3. The same as in Fig. 2, but for the neutron single-particle spectrum.

particle spectrum at the saddle is quite uniform and this is why the shell correction energy is expected to be rather small.

We obtain an even more complicated picture of single-particle states after diagonalization of the deformed Woods-Saxon potential for neutrons. A sufficiently wide energy gap at $N = 184$ is confirmed at the ground state. There is smaller but clear energy gap at $N = 178$. The single-particle spectrum is denser for neutrons than that for protons.

B. Level-density parameter

The comparisons of energy dependencies of the level-density parameter $a(A, U)$ from the fit of the calculated level densities with Eq. (12) and those obtained from Eq. (13) are presented in Fig. 4 for ^{292}Fl , ^{296}Lv , and $^{300}\text{120}$ nuclei. As seen, there is a very good agreement of these dependencies at $U \geq 15$ MeV. Analyzing mass number dependence of the asymptotic level density parameters with Eq. (14), we find the coefficients $\alpha = 0.09 \text{ MeV}^{-1}$, $\beta = 2.89 \times 10^{-5} \text{ MeV}^{-1}$ for the ground state [see Fig. 5(a)]. These values are close to those obtained in Ref. [35]. Damping parameters calculated independently for every nuclear systems at the ground states are shown in Fig. 5(b). Despite the rather scattered nature of this parameter for use in Eq. (13), one can try still to find a universal value for E_D . As found, the ground-state damping parameters are in average close to $E_D \approx 15$ MeV. Our results in Fig. 5(b) show that in the nuclei considered the value of E_D can be calculated with Eq. (15) taking $\gamma_0 = 0.423 \text{ MeV}^{-1}$.

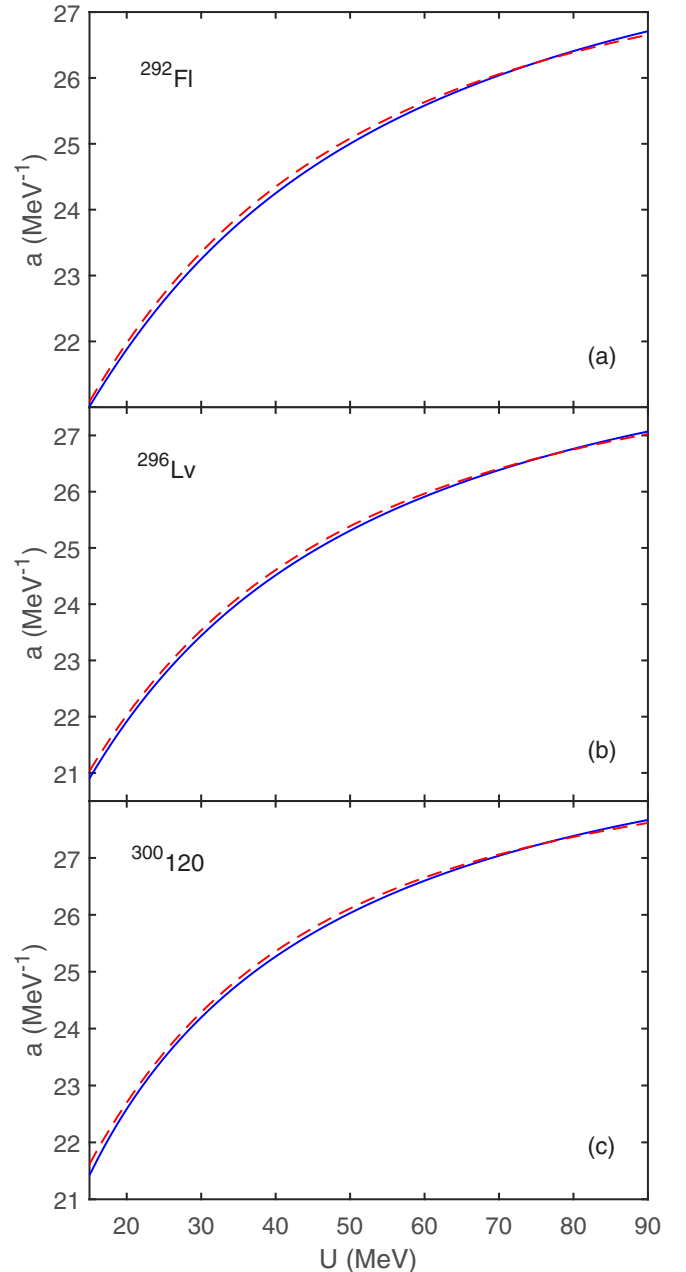


FIG. 4. Comparison of energy dependencies of the ground-state level-density parameters obtained by fitting the calculated level densities (11) with the Fermi-gas expression (12) at the ground state (solid lines) and those obtained with the phenomenological expression (13) (dashed lines) for nuclei ^{292}Fl (a), ^{296}Lv (b), and $^{300}\text{120}$ (c).

This value is close to that obtained in Ref. [36] from the analysis of neutron resonance densities and low-lying nuclear levels.

In Fig. 6, the energy dependencies of the saddle-point a calculated for ^{292}Fl , ^{296}Lv , and $^{300}\text{120}$ are compared with the phenomenological model (13). At the saddle point, the shell corrections are rather small or even close to zero and, thus, Eq. (13) is unsuitable to describe the calculated values of $a(A, U)$. Replacing the pure shell correction, taken as indicated just from the diagonalization of the deformed

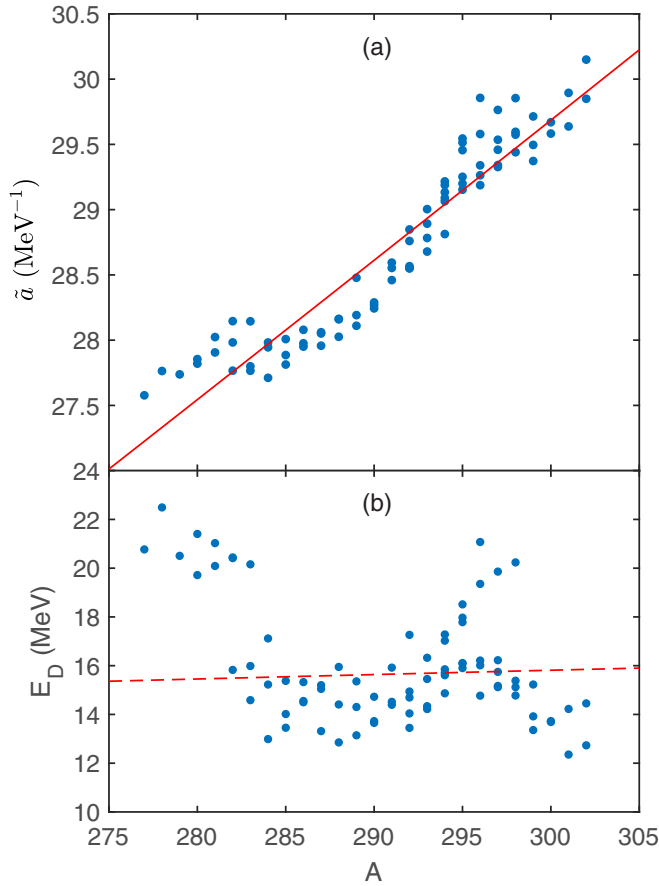


FIG. 5. (a) Mass number dependence of the asymptotic ground-state level-density parameter $\tilde{a}(A)$ obtained with the phenomenological expression (13) (symbols). The fit of $\tilde{a}(A)$ with Eq. (14) is shown by the solid line. (b) The corresponding damping parameters (symbols) in Eq. (13) are approximated by $E_D = A^{1/3}/0.423$ (dashed line).

Woods-Saxon potential in Eq. (13) by $(\delta E_{sh} - \Delta_N - \Delta_Z)$, we have much better agreement with the results of direct calculations. This supports the idea of considering damping of both pairing and shell effects at the saddle point where these effects are comparable. We obtain the following coefficients: $\alpha = 0.122 \text{ MeV}^{-1}$ and $\beta = -7.3 \times 10^{-5} \text{ MeV}^{-1}$ in the mass dependence (14) of \tilde{a} . It should be noted that, as in the case of the ground state, we got practically linear dependence of the parameter \tilde{a} with mass number, as β is only of the order of $\approx 10^{-5}$ in both ground state and saddle points. Comparison between the values of \tilde{a} at the saddle point with the result of Eq. (14) is shown in Fig. 7(a). Damping parameters calculated independently for every nuclear systems at saddle points are shown in Fig. 7(b). As seen in Fig. 7(b), the saddle-point damping parameters are close to $E_D \approx 17 \text{ MeV}$ for $A < 290$. Though the formal fit results in small value of E_D at the saddle point for $A > 290$, in the calculation of the survival probability one can use larger E_D because the shell effects at the saddle points are small in these nuclei and their damping rate weakly influences the level density parameter in accordance with Eq. (13). Indeed, if the value of $|\delta E_{sh}|$ is small, then the

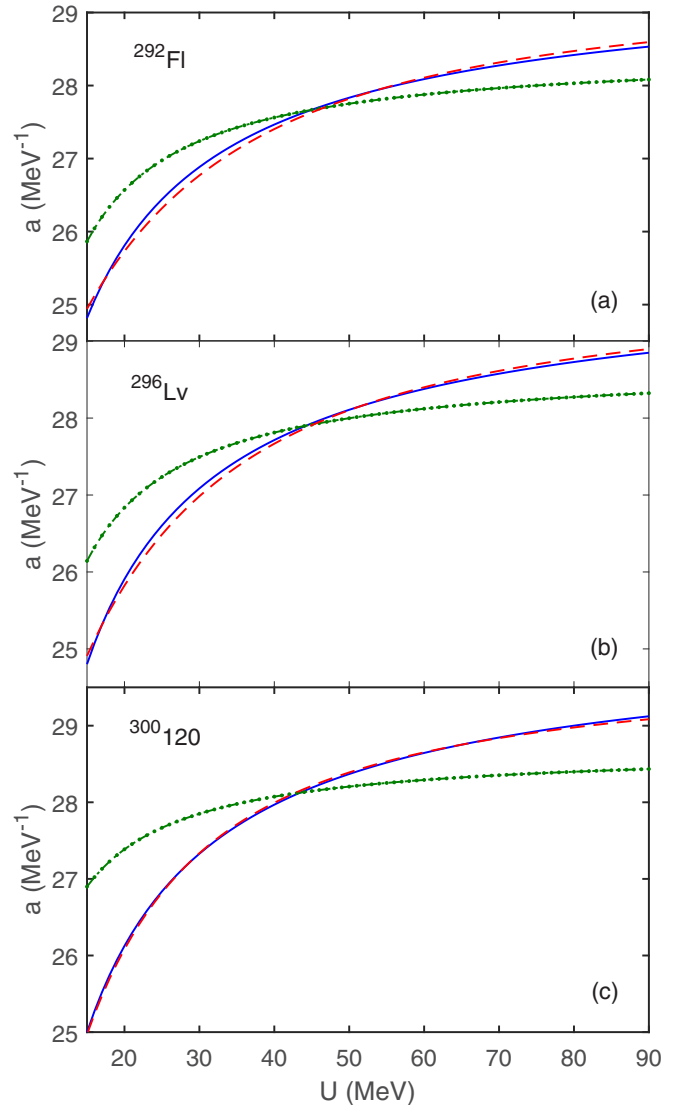


FIG. 6. The same as in Fig. 4, but for the saddle point. The calculated values of a (solid lines) are compared with those from the phenomenological expression (13) with (dashed lines) and without (dash-dotted lines) replacement of the shell correction δE_{sh} by $\delta E_{sh} - \Delta_Z - \Delta_N$.

second term in the parentheses in Eq. (13) is much smaller than unity.

The ratio $a_{\text{SP}}(A, U - B_f)/a_{\text{GS}}(A, U)$ of the level-density parameter at the saddle point to that at the ground state is shown in Fig. 8(a) for the $Z = 114$ isotopic chain at various excitation energies U . The shell effects, which are evident in the a ratios at $U \geq 20 \text{ MeV}$, decrease at higher energies. In Fig. 8(b), the shell effects ($U = 0$) are presented at the ground state (solid line) and saddle point (dashed line) for various Fl isotopes. Though the shell effects at the ground state are of most importance, they cannot be disregarded at the saddle point. So, the *topographic theorem* [37], that the shell effects disappear at the saddle point and the fission barrier is just equal to the shell energy as the nucleus possesses at the ground state, is only approximately valid for superheavy nuclei.

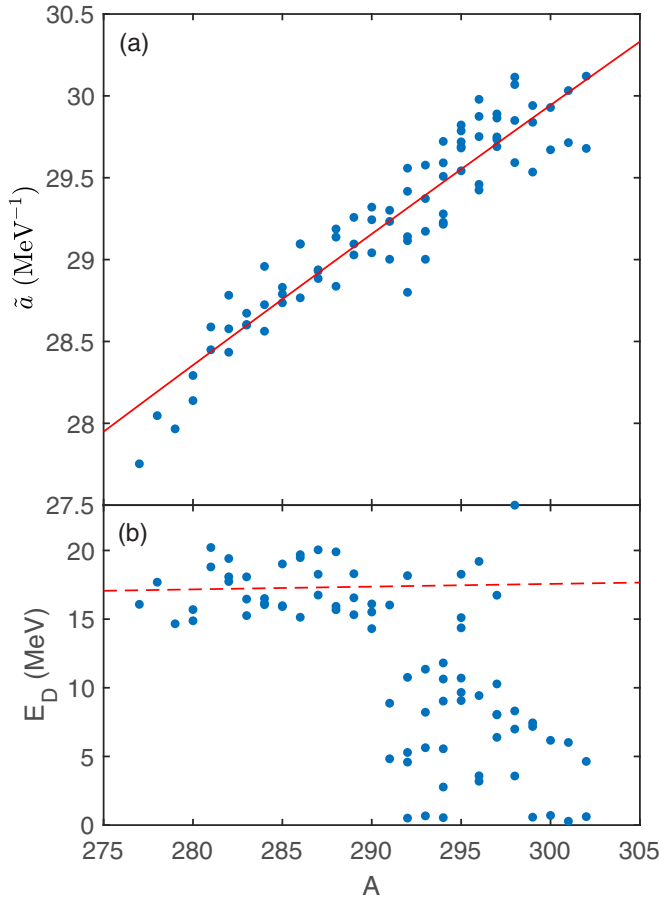


FIG. 7. The same as in Fig. 5, but for the asymptotic saddle-point level-density parameter $\tilde{a}(A)$ and the saddle-point damping parameter E_D . Here, the damping parameters are approximated by $E_D = A^{1/3}/0.381$ (dashed line) for $A < 290$.

C. Fission and neutron emission probabilities

Because the statistical approach is used here, the details of the fission path variability between extremes are not that important. Only the thresholds that prohibit specific decay are required: the separation energy with the mass of daughter nucleus for decay via neutron emissions and the height of fission barrier.

To validate our calculations of the level densities, first we compare the calculated fission probabilities $\Gamma_f/\Gamma_{\text{tot}}$ for ^{236}U and ^{240}Pu with the available experimental data. In Fig. 9, the energy dependence of $\Gamma_f/\Gamma_{\text{tot}}$ calculated with Eqs. (16)–(18) is shown for ^{236}U and ^{240}Pu together with the experimental data from Ref. [38]. In this calculation the values of B_n are obtained from the experimental binding energies and the B_f values are taken as the experimental highest fission saddles, i.e., the first saddle for ^{240}Pu [39] and second saddle for ^{236}U [36]. As seen, the expression (17) gives results close to those of the numerical calculations with Eq. (16). A good agreement with the empirical values seen in Fig. 9 gives us confidence for the reliable predictions of fission and neutron emission probabilities in the region of heavy nuclei. The values of B_n and B_f calculated in Ref. [31] result in $\Gamma_f/\Gamma_{\text{tot}}$

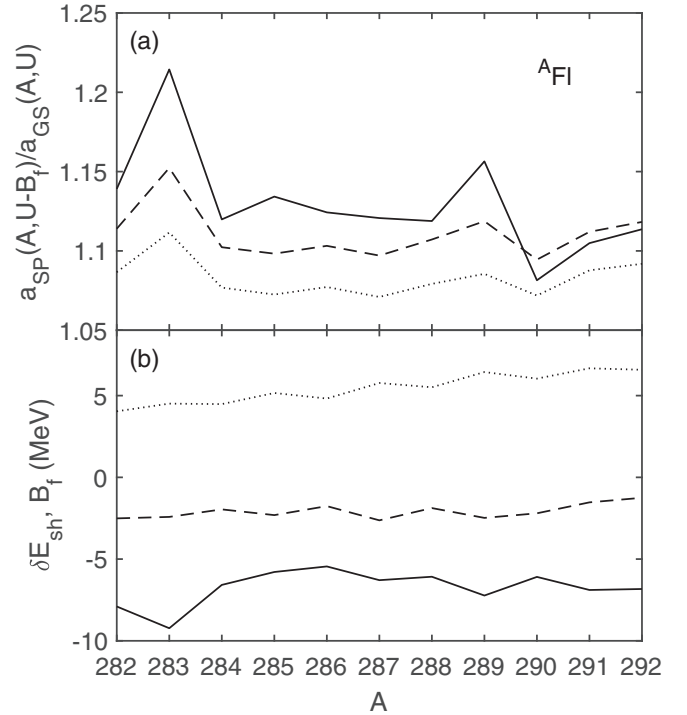


FIG. 8. For ^AFI isotopes, (a) the ratios of the level density parameters at the saddle point and ground state are shown at the excitation energies 20 MeV (solid line), 40 MeV (dashed line), and 60 MeV (dotted line). At the saddle point the excitation energy is decreased by the high B_f of the fission barrier. (b) The values of shell corrections at the ground state (solid line) and the ones at the saddle point (dashed line), and the heights of fission barriers (dotted line) are presented as functions of mass number A at zero excitation energy.

values which are less, within the factor of 2, but just as dependent on energy. At $U > 25$ MeV, the difference is about 10–20%.

In the spirit of canonical transition-state theory (TST) [40] the probability ratio for two selected decay types (transitions) is proportional to the number of states available for each of them in the appropriate energy range (saturating total available energy). This means that the excitation energy dependence of Γ_n/Γ_f is strongly affected by the difference between the fission barrier height and neutron binding energy; see schematic Fig. 10.5 in [41] or Fig. 9 in [42]. Application of TST in practice can be found, e.g., in [42–45]. As seen from Eq. (16), at $a_f \approx a_n$ an increasing Γ_n/Γ_f with the excitation energy is expected at $(B_f + \Delta_f) - (B_n + \Delta_n) < 0$, and the opposite trend is expected at $(B_f + \Delta_f) - (B_n + \Delta_n) > 0$. However, our calculations show that, in the nuclei considered, the a_f values are on average ≈ 10 – 30% larger than a_n . Because of the exponential nature of the survival probability (17), the ratio a_f/a_n strongly affects the ratio Γ_n/Γ_f . The calculated ratios a_f/a_n for $Z = 117$ and $Z = 120$ isotopic chains are shown in Fig. 10 for various excitation energies, together with the corresponding phenomenological results obtained with Eq. (13). As seen, the shell and pairing effects decrease with excitation energy and ratios a_f/a_n reach

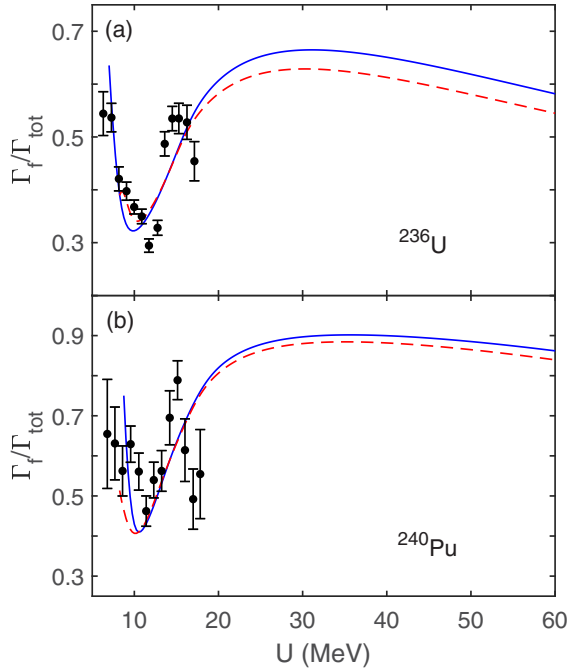


FIG. 9. The dependence of fission probability $\Gamma_f/\Gamma_{\text{tot}}$ on excitation energy for the fissioning nuclei ^{236}U (a) and ^{240}Pu (b). The results obtained with Eq. (16) (blue solid line) and analytical expression (17) (red dashed line) are compared with the experimental data (symbols) from Ref. [38].

asymptotic values more or less equal to 1.1. As a consequence of the disappearance of quantum effects, the visible strong staggering of a_f/a_n weakens significantly with excitation. One can also see that the approximate formula [Eq. (13)] works very well in the whole range of excitation energy for all considered nuclei.

The dependence of a_f/a_n on excitation energy for ^{284}Fl (green solid line), ^{288}Fl (red dot-dashed line), and ^{292}Fl (blue dashed line) isotopes is shown in Fig. 11. In all presented Fl cases a_f/a_n values clearly deviate from 1; for example for ^{284}Fl at maximum it is about 1.35. The course of variability of this ratio as a function of excitation energy is similar in all three flerovium nuclei. At first it grows quite quickly to reach a maximum of about 20 MeV and then slowly falls. Only for very high excitation energies do the curves saturate to an asymptotic value less than 1.1.

In Fig. 12, the energy dependence of neutron emission probability is shown for ^{278}Cn , ^{294}Og , and $^{296,298}120$. As follows from the expression (17), the general increase of $\Gamma_n/\Gamma_{\text{tot}}$ with the excitation energy for ^{278}Cn and $^{296,298}120$ is due to positive values of the derivative of the exponential part, $\sqrt{a_n}/(U - B_n - \Delta_n) - \sqrt{a_f}/(U - B_f - \Delta_f) > 0$. Similarly, the condition $\sqrt{a_n}/(U - B_n - \Delta_n) - \sqrt{a_f}/(U - B_f - \Delta_f) < 0$ for the ^{294}Og [Fig. 12(b)] nucleus leads to a decrease of $\Gamma_n/\Gamma_{\text{tot}}$ with increasing excitation energy. These exact numerical results are shown in Fig. 12 by solid blue lines. Note that depending on the superheavy system the scale of $\Gamma_n/\Gamma_{\text{tot}}$ is different. The local variations seen in $\Gamma_n/\Gamma_{\text{tot}}$ curves at lower energies

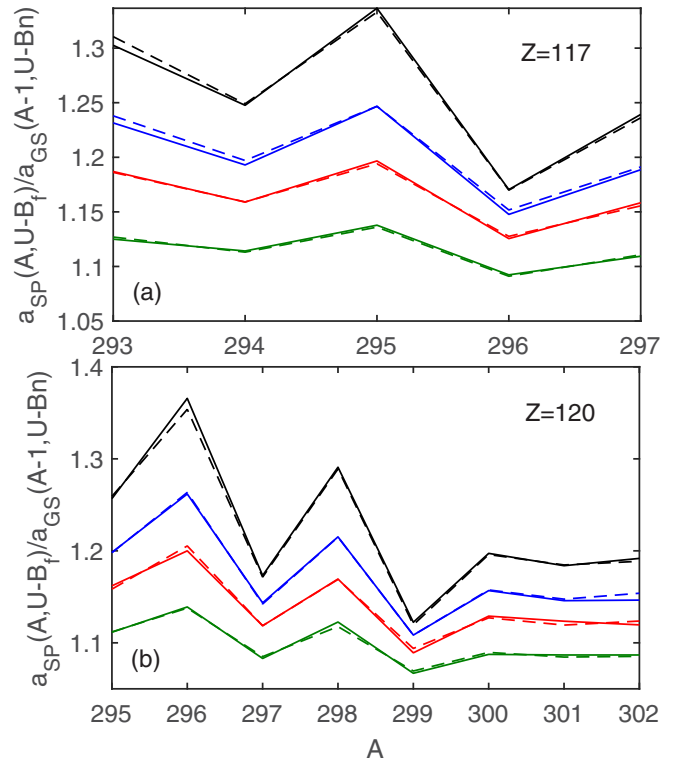


FIG. 10. For $Z = 117$ (a) and $Z = 120$ (b) isotopic chains, the ratios of the level density parameter of the mother nucleus at the saddle point to that of the daughter nucleus after neutron separation at the ground state at $U = 25$ (solid black line), 35 (solid blue line), 45 (solid red line), and 65 MeV (solid green line). The corresponding phenomenological results of Eq. (13) are shown by dashed lines.

may be caused by the already discussed strong shell and pairing effects in a_f/a_n . This study proves how important and even decisive is the role of energy dependent level-density parameters at the saddle point and ground state. We have shown that the phenomenological expression (13) seems to

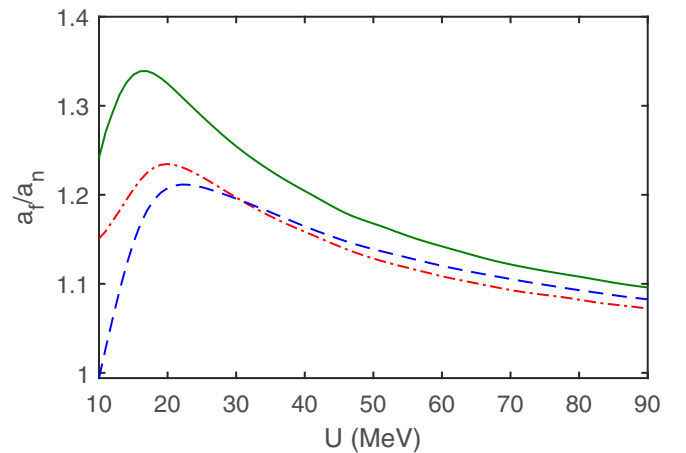


FIG. 11. The dependencies of a_f/a_n (19) on excitation energy for ^{284}Fl (green solid line), ^{288}Fl (red dot-dashed line), and ^{292}Fl (blue dashed line).

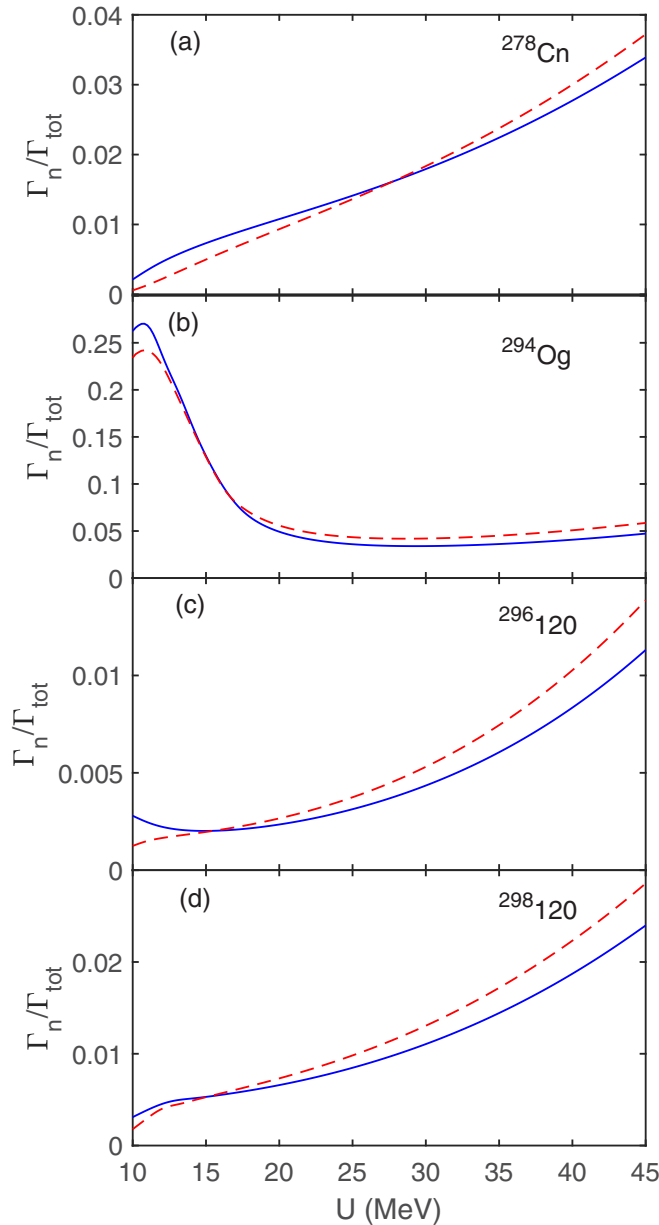


FIG. 12. The dependence of neutron emission probability on excitation energy for ^{278}Cn (a), ^{294}Og (b), $^{296}_{120}$ (c), and $^{298}_{120}$ (d). The increasing trend for ^{278}Cn and $^{296,298}_{120}$ nuclei and decreasing trend for the ^{294}Og nucleus are in agreement with the positive or negative sign of the derivative of the exponential part in (17). Numerical calculations are shown by blue solid lines and the results of expression (17) are depicted by red dashed lines.

be suitable for Eq. (17) to describe the energy dependence of $\Gamma_n/\Gamma_{\text{tot}}$. Results of these approximate calculations are shown by red dashed lines in Fig. 12. Only for $Z = 120$ do both results vary noticeably for very large excitation energy values, which, however, are not important to us here.

IV. CONCLUSIONS

Since, the nuclear level density is of special importance for the cross section calculations and nuclear structure studies

in general, we devoted this article to this quantity. It takes on special significance for superheavy nuclei in which we are dealing with extremely low probabilities of their production. The level-density parameter was evaluated here by fitting of obtained numerical and exact results to the well known Fermi gas expression. The single-particle energies were calculated within the microscopic-macroscopic model based on the diagonalization of the deformed single-particle Woods-Saxon potential. The Yukawa-plus exponential model for macroscopic energy calculation was used. We carried out our analysis not only for the ground states but also for the saddle points, which is new in these kinds of calculations. The energy and shell correction dependencies of the level-density parameter of superheavy nuclei at these extremes were studied and compared with the well-known Ignatyuk expression.

The following conclusions can be drawn:

(i) We have shown that a phenomenological approach based on the Ignatyuk formula agrees well when one calculates energy dependence of the level-density parameter at the ground state and strongly disagrees, particularly for small excitation energies, at the saddle point configurations. Thus, Eq. (13) cannot be safely used for the saddle at low excitation energies.

(ii) The investigated ratio of the level-density parameter at the saddle point to that at the ground state, which is a very important factor in evaluation of the probability of fission, in comparison to the probability of neutron emissions, is far from unity, especially for not too hot nuclear systems.

(iii) As shown, the “topographic theorem” can be applied with some caution to nuclei having a substantial saddle point shell correction.

(iv) We also note a substantial difference in average level-density parameters between mother nucleus at saddle point and daughter nucleus after neutron emission, with a distinct staggering effect visible at the same time. Having nuclear level densities at saddles and ground states, one can directly or numerically evaluate competition between neutron emission and fission. Numerically determined damping parameters have a weaker effect on the saddle point compared to the ground state.

With the obtained $\Gamma_n/\Gamma_{\text{tot}}$ one can calculate the survival probabilities of excited superheavy nuclei without involving any free parameters. Indeed the binding energies, fission thresholds, shells corrections, and finally level densities calculated on the same basis are quite important.

ACKNOWLEDGMENTS

The work of M.K. was cofinanced by the National Science Centre under Contract No. UMO-2013/08/M/ST2/00257 (LEA COPIGAL). T.M.S, G.G.A., and N.V.A. were supported by the Ministry of Science and Higher Education of the Russian Federation (Moscow, Contract No. 075-10-2020-117). A.N.B. was partly supported by RFBR (Grant No. 20-02-00176).

- [1] Yu. Ts. Oganessian and V. K. Utyonkov, *Nucl. Phys. A* **944**, 62 (2015).
- [2] Yu. Ts. Oganessian and K. P. Rykaczewski, *Phys. Today* **68**(8), 32 (2015).
- [3] S. Hilaire, J. P. Delaroche, and M. Girod, *Eur. Phys. J. A* **12**, 169 (2001).
- [4] S. Goriely, S. Hilaire, and A. J. Koning, *Phys. Rev. C* **78**, 064307 (2008).
- [5] A. H. Blin *et al.*, *Nucl. Phys. A* **456**, 109 (1986).
- [6] H. Uhrenholt, S. Åberg, A. Dobrowolski, Th. Døssing, T. Ichikawa, and P. Möller, *Nucl. Phys. A* **913**, 127 (2013).
- [7] S. Åberg, B. G. Carlsson, Th. Døssing, and P. Möller, *Nucl. Phys. A* **941**, 97 (2015).
- [8] D. E. Ward, B. G. Carlsson, Th. Døssing, P. Möller, J. Randrup, and S. Åberg, *Phys. Rev. C* **95**, 024618 (2017).
- [9] M. Albertsson, B. G. Carlsson, Th. Døssing, P. Möller, J. Randrup, and S. Åberg, *Phys. Lett. B* **803**, 135276 (2020).
- [10] B. Nerlo-Pomorska, K. Pomorski, J. Bartel, and K. Dietrich, *Phys. Rev. C* **66**, 051302(R) (2002).
- [11] J. Bartel, K. Pomorski, and B. Nerlo-Pomorska, *Int. J. Mod. Phys. E* **15**, 478 (2006).
- [12] B. Nerlo-Pomorska, K. Pomorski, J. Bartel, and A. Dobrowolski, *Acta Phys. Pol. B* **39** (2008).
- [13] R. A. Senkov and M. Horoi, *Phys. Rev. C* **82**, 024304 (2010).
- [14] Y. Alhassid, M. Bonett-Matiz, S. Liu, and H. Nakada, *Phys. Rev. C* **92**, 024307 (2015).
- [15] Yu. V. Sokolov, *Level Densities of Atomic Nuclei* (Energoizdat, Moscow, 1990).
- [16] A. B. Ignatyuk and G. N. Smirenkin, and A. S. Tishin, *Yad. Fiz.* **21**, 485 (1975).
- [17] P. Decowski, W. Grochulski, A. Marcinkowski, K. Siwek, and Z. Wilhelmi, *Nucl. Phys. A* **110**, 129 (1968).
- [18] V. M. Strutinski, *Sov. J. Nucl. Phys.* **3**, 449 (1966); *Nucl. Phys. A* **95**, 420 (1967).
- [19] S. Ćwiok, J. Dudek, W. Nazarewicz, J. Skalski, and T. Werner, *Comput. Phys. Commun.* **46**, 379 (1987).
- [20] H. J. Krappe, J. R. Nix, and A. J. Sierk, *Phys. Rev. C* **20**, 992 (1979).
- [21] I. Muntian, Z. Patyk, and A. Sobiczewski, *Acta Phys. Pol. B* **32**, 691 (2001).
- [22] M. Kowal, P. Jachimowicz, and A. Sobiczewski, *Phys. Rev. C* **82**, 014303 (2010).
- [23] P. Jachimowicz, M. Kowal, and J. Skalski, *Phys. Rev. C* **89**, 024304 (2014).
- [24] P. Jachimowicz, M. Kowal, and J. Skalski, *Phys. Rev. C* **95**, 034329 (2017).
- [25] W. D. Myers and W. J. Swiatecki, *Nucl. Phys. A* **601**, 141 (1996).
- [26] P. Möller and A. Iwamoto, *Phys. Rev. C* **61**, 047602 (2000).
- [27] P. Möller, A. J. Sierk, T. Ichikawa, A. Iwamoto, R. Bengtsson, H. Uhrenholt, and S. Aberg, *Phys. Rev. C* **79**, 064304 (2009).
- [28] P. Jachimowicz, M. Kowal, and J. Skalski, *Phys. Rev. C* **85**, 034305 (2012).
- [29] A. Mamdouh, J. M. Pearson, M. Rayet, and F. Tondeur, *Nucl. Phys. A* **644**, 389 (1998).
- [30] P. Jachimowicz, M. Kowal, and J. Skalski, *Phys. Rev. C* **95**, 014303 (2017).
- [31] P. Jachimowicz, M. Kowal, and J. Skalski, *Phys. Rev. C* **101**, 014311 (2020).
- [32] P. Jachimowicz, M. Kowal, and J. Skalski, *At. Data Nucl. Data Tables*, **138**, 101393 (2021).
- [33] G. D. Adeev and P. A. Cherdantsev, *Yad. Fiz.* **21**, 491 (1975).
- [34] R. Vandenbosch and J. R. Huizenga, *Nuclear Fission*, (Academic, New York, 1973).
- [35] A. N. Bezbakh, T. M. Shneidman, G. G. Adamian, and N. V. Antonenko, *Eur. Phys. J. A* **50**, 97 (2014).
- [36] R. Capote *et al.*, *Nucl. Data Sheets* **110**, 3107 (2009).
- [37] W. J. Swiatecki, *Phys. Rev.* **100**, 937 (1955).
- [38] E. Cheifetz, H. C. Britt, and J. B. Wilhelmy, *Phys. Rev. C* **24**, 519 (1981).
- [39] G. N. Smirenkin, IAEA Report No. INDC(CCP)-359, Vienna, 1993 (unpublished).
- [40] P. Hänggi, P. Talkner, and M. Borkovec, *Rev. Mod. Phys.* **62**, 251 (1990).
- [41] P. Fröbrich and R. Lipperheide, *Theory of Nuclear Reactions* (Oxford University, New York, 1996).
- [42] W. J. Swiatecki, K. Siwek-Wilczyńska, J. Wilczyński, *Phys. Rev. C* **71**, 014602 (2005).
- [43] W. J. Swiatecki, K. Siwek-Wilczyńska, J. Wilczyński, *Acta Phys. Pol. B* **34** (2003).
- [44] K. Siwek-Wilczyńska, T. Cap, M. Kowal, A. Sobiczewski, and J. Wilczyński, *Phys. Rev. C* **86**, 014611 (2012).
- [45] K. Siwek-Wilczyńska, T. Cap, and M. Kowal, *Phys. Rev. C* **99**, 054603 (2019).